Environmental Challenges 4 (2021) 100109

Contents lists available at ScienceDirect

Environmental Challenges

journal homepage: www.elsevier.com/locate/envc

CO_2 sorption using encapsulated imidazolium-based fluorinated ionic liquids

Franciele L. Bernard[a], Evandro A. Duarte[a], Barbara B. Polesso[b], Rafael B. Duczinski[b], Sandra Einloft[a,b,*]

[a] School of Technology, Pontifical Catholic University of Rio Grande do Sul - PUCRS, Porto Alegre Brazil
[b] Post-Graduation Program in Materials Engineering and Technology, School of Technology Pontifical Catholic University of Rio Grande do Sul – PUCRS, Brazil

ARTICLE INFO

Keywords':
CO_2 capture
Encapsulated ionic liquid
Microcapsules
Ionic liquid

ABSTRACT

The development and testing of new sorbents for the efficient removal of CO_2 from flue gases is essential. Encapsulated room-temperature ionic liquids (RTILs) can be potentially employed in CO_2 capture. In this work, we report the preparation and characterization of encapsulated imidazolium-based fluorinated RTILs for CO_2 capture. [Emim][TF_2N], [Bmim][TF_2N], and [Hmim][TF_2N] RTILS were encapsulated in polysulfone (PSF) using an emulsification method and characterized by several techniques. The pressure-decay technique was used to assess the CO_2 sorption capacity and reusability. Encapsulated RTILs showed improved utility for CO_2 capture processes compared with non-encapsulated RTILs, including higher CO_2 sorption capacity and faster CO_2 sorption/desorption. The CO_2 absorption/desorption cycles demonstrated the reuse capacity of all microcapsules under mild conditions. The highest CO_2 sorption capacity was noted for encapsulated [Emim][TF_2N] (39.5 mg CO_2 g^{-1} at 298.15 K and 1 bar; 62.7 mg CO_2 g^{-1} at 298.15 K and 10 bar). It is worth emphasizing that the encapsulated [Emim][TF_2N] contained a lower ionic liquid (IL) content (37.5. ± 0.6) when compared to other encapsulated samples. Moreover, encapsulated [Emim][TF_2N] presented a higher CO_2 affinity than the encapsulated ILs reported in the literature.

1. Introduction

Global CO_2 emissions are increasing annually. Continuous rise in CO_2 emissions will severely hinder the aim of the Paris Climate Agreement for maintaining the increase in global average temperatures below 2 °C (275.15 K) compared to the pre-industrial levels; the goal to maintain the temperature increase below 1.5 °C (274.65 K) would be even harder to achieve. The measurements carried out at the Mauna Loa Observatory (MLO), Hawaii show an increase in CO_2 concentration by approximately 48% (415.09 ppm) when compared to the pre-industrial levels of 280 ppm (Gudoshava et al., 2020; "Mauna Loa Observatory, Hawaii. Last diagram update: " 2020; Shiogama et al., 2020).

Carbon capture and storage (CCS) technologies can help countries meet their goals and decrease global warming (Anwar et al., 2018; Ketzel et al., 2015; Roefs et al., 2019; Wilberforce et al., 2019), as CCS technologies can capture over 90% of CO_2 emissions produced from stationary energy sources (Wilberforce et al., 2019). The three main routes used for CO_2 capture are post-combustion, pre-combustion, and oxyfuel (Ağralı et al., 2018; Borhani et al., 2015; Olajire, 2010).

The most mature CO_2 capture process is chemical absorption using aqueous alkanolamine solutions such as monoethanolamine (MEA), diethanolamine (DEA), triethanolamine (TEA), and methyl diethanolamine (MDEA). The use of these compounds in the capture process presents some drawbacks, including amine degradation/evaporation, equipment corrosion, and a high energy penalty for absorbent regeneration (McGurk et al., 2017; Yu, 2012). Therefore, the development of new solid sorbents for CO_2 capture is essential in the CCS field.

Different types of materials have been investigated for CO_2 capture, such as room-temperature ionic liquid (RTIL)(Anthony et al., 2002a; Camper et al., 2004), poly(ionic liquid)s (PILs)(Bernard et al., 2016; Franciele L. Bernard et al., 2019a; Sadeghpour et al., 2016; Tang et al., 2005; Zulfiqar et al., 2015), ionic liquids immobilized in mesoporous silica (Duczinski et al., 2020), supported ionic liquid membranes (SILMs)(Hanioka et al., 2008; Zhang et al., 2019), cellulose-based sorbents (Franciele L. Bernard et al., 2019b; Franciele Longaray Bernard et al., 2019; Hernández et al., 2020), and azole-based protic ionic liquids (PILs)(Zhang et al., 2020).

* Corresponding author at: School of Technology, Pontifical Catholic University of Rio Grande do Sul - PUCRS, Porto Alegre, Brazil.
E-mail address: einloft@pucrs.br (S. Einloft).

https://doi.org/10.1016/j.envc.2021.100109
Received 1 March 2021; Received in revised form 24 March 2021; Accepted 9 April 2021

In recent years, encapsulated liquid sorbents have also been proposed as an option for CO_2 capture (Einloft and Bernard, 2020). RTIL encapsulation has been identified as a new development trend for improving CO_2 uptake and overcoming the drawbacks of non-encapsulated RTILs and aqueous alkanolamine solutions (Einloft and Bernard, 2020; Stolaroff et al., 2016).

Solvent encapsulation may promote a faster CO_2 sorption rate and better sorption capacity than non-encapsulated solvents by increasing the specific surface area and by promoting solvent isolation inside the polymeric shell, preventing solvent contact with the sorption facility and gas stream (Einloft and Bernard, 2020; Stolaroff et al., 2016). The use of non-aqueous solvents may reduce the cost of CO_2 capture, mainly because of the lack of equipment corrosion and lower regeneration energy requirements over existing aqueous alkanolamine systems (Nie et al., 2018).

RTILs are an essential class of green solvents with unique characteristics such as high thermal stability, negligible vapor pressure, non-flammability, tenability, and high selectivity for CO_2 (Hasib-ur-Rahman et al., 2010). However, their high viscosity and price are drawbacks that hamper the implementation of non-encapsulated RTILs in CO_2 separation processes (Farahipour and Karunanithi, 2014).

Currently, there are few studies on the application of encapsulated RTILs for CO_2 uptake. However, numerous publications have described the potential of non-encapsulated RTILs for use in CO_2 capture systems (Bai et al., 2017; Hasib-ur-Rahman et al., 2010; Sarmad et al., 2017; Zeng et al., 2017). RTILs based on alkylimidazolium cations have been investigated for CO_2 capture applications (Anthony et al., 2005, 2002b; Bai et al., 2017; Blanchard et al., 2001; Brennecke and Gurkan, 2010; Cadena et al., 2004; Privalova et al., 2012). Increased CO_2 solubility in RTILs may be achieved using fluorinated anions such as bis(trifluoromethylsulfonyl)imide ([Tf_2N]) and tris(trifluoromethylsulfonyl)methide ([*methide*]) (Aki et al., 2004).

The literature also reports the effect of RTIL cations on CO_2 solubility (Condemarin and Scovazzo, 2009; Ferguson and Scovazzo, 2007; Hou and Baltus, 2007; Sarmad et al., 2017; Shannon et al., 2012; Shiflett and Yokozeki, 2005). The augmentation of the cation alkyl-side chain improves CO_2 affinity because it increases the available free volume for CO_2 with a corresponding decrease in cation-anion interactions (Hou and Baltus, 2007; Shannon et al., 2012; Shiflett and Yokozeki, 2005).

Recently, Kaviani et al. (2018a) reported the encapsulation of imidazolium-based fluorinated RTILs (1-ethyl-3-methylimidazolium bis(trifluoromethylsulfonyl)imide ([E*mim*][TF_2N]) and 1-hexyl-3-methylimidazolium bis(trifluoromethylsulfonyl)imide ([H*mim*][TF_2N])) within a fluoropolymer shell (poly(vinylidene fluoride-cohexafluoropropylene-PVDF-HFP) by a single-step non-solvent-induced phase separation method. Capsules with diameters ranging from 1000 to 2000 μm were produced. Microcapsules of fluorinated RTILs exhibited higher CO_2 capture capacity and recyclability than non-encapsulated RTILs, demonstrating their potential for use in CO_2 capture processes.

Herein, we report the encapsulation of different fluorinated imidazolium-based RTILs, including 1-Ethyl-3-methylimidazolium bis(trifluoromethylsulfonyl)imide ([E*mim*][TF_2N]), 1-Butyl-3-methylimidazolium bis(trifluoromethylsulfonyl)imide ([B*mim*][TF_2N]), and 1-Hexyl-3-methylimidazolium bis(trifluoromethylsulfonyl)imide ([H*mim*][TF_2N]) in polysulfone (PSF) by means of an emulsification method. We studied the effect of the alkyl side chain length of imidazolium cations (C_2, C_4, and C_6) containing TF_2N anions on the morphology, thermal stability, encapsulation capacity (RTIL%), and CO_2 sorption capacity of the encapsulated RTIL. CO_2 sorption/desorption cycles were used to assess the recyclability of the encapsulated RTILs. The CO_2 sorption capacity of the encapsulated RTIL compared with that of both the non – encapsulated RTIL and polysulfone samples was also evaluated.

2. Experimental section

2.1. Materials

1-Methylimidazole (≥99%, Sigma-Aldrich), 1-chlorobutane (99%, Sigma-Aldrich), bromoethane (98%, Sigma-Aldrich), 1-chlorohexane (99%, Sigma-Aldrich), acetonitrile (P.A, Synth), bis (trifluoromethylsulfonyl)amine lithium salt (99.95%, Sigma-Aldrich), polysulfone (average Mw ~35,000 by LS, average Mn ~16,000 by MO, pellets, Sigma-Aldrich), dichloromethane (P.A, Synth), and gelatin (Sigma-Aldrich).

2.2. [C_n*mim*][TF_2N] synthesis

1-Ethyl-3-methylimidazolium bis(trifluoromethylsulfonyl)imide ([EMIM][TF_2N]), 1-Butyl-3-methylimidazolium bis(trifluoromethyl sulfonyl)imide ([B*mim*][TF_2N]) and 1-Hexyl-3-methylimidazolium bis(trifluormethylsulfonyl)imide ([H*mim*][TF_2N]) RTILs were synthesized following procedures adapted from literature(Freire et al., 2008; Jairton et al., 2002; Zhang et al., 2021) (Fig. S1). Firstly, 1-alkyl-3-methylimidazolium chloride ([$C_n$mim] [Cl], n = 2,4 or 6), was synthesized in a three-necked flask at 353.15–363.15 K over 24 h using 0.1 mol of 1-methylimidazole and 0.15 mol of 1-chlorobutane (Bromoethane or 1-chlorohexane) in acetonitrile. [$C_n$mim] [Cl] was filtered, and the volatile material was removed under vacuum (10^{-3} mbar). Then, 0.1 mol of [$C_n$mim] [Cl] and 0.1 mol of bis (trifluoromethylsulfonyl)amine lithium salt was dissolved in distilled water in a three-necked flask. The reaction mixture was stirred at room temperature for 24 h. The liquid reaction mixture split into two immiscible phases: upper phase (water) and lower phase (RTIL). A separatory funnel was used to separate immiscible phases. When the upper phase (water) was removed from the separatory funnel, RTIL was washed several times with distilled water until no chloride could be detected. Ultimately, the RTIL was dried at 353 K for 48 h under vacuum (10^{-3} mbar) to produce [$C_n$mim][TF_2N] hydrophobic RTIL (Freire et al., 2008). The water content of [$C_n$mim][TF_2N] RTILs, measured by Karl Fischer method (SI Analytics model Tritoline KF-trace), is approximately 1022 ppm (0.1 wt%). RTIL structures were confirmed using the Proton Nuclear Magnetic Resonance (^{1}H NMR) spectroscopic technique in DMSO-d_6 (Bruker Avance DRX-400 spectrometer at 400 MHz) and from Fourier-transform infrared (FTIR) spectra. The ^{1}H NMR spectrum analysis confirmed the structures of all synthesized RTILs (Fig. S2). [Emim][TF_2N]: ^{1}H NMR (400 MHz, $CDCl_3$) δ ppm: 1.48 (t, 3H), 3.96 (s, 3H), 4.16 (m, 2H), 7.29 (s, 1H), 7.35 (s, 1H) and 8.52 (s, 1H). [Bmim][TF_2N] (Fig. 4.1b): ^{1}H NMR (400 MHz, $CDCl_3$) δ ppm: 0.96 (3H, t, -CH_3), 1.35 (2H, m, -C**H**$_2$-CH_3), 1.85 (2H, m, -CH_2-C**H**$_2$-CH_2), 3.9 (3H, s, C**H**$_3$-N), 4.16 (2H, t, -N-C**H**$_2$-CH_2), 6.90 (1H, s, -C**H**), 7.03 (1H, s, -C**H**) and 8.7 (1H, s, -C**H**)(Kurnia et al., 2017; Rao and Gejji, 2016). [Hmim][TF_2N] (Fig. 4.1c): ^{1}H NMR (400 MHz, $CDCl_3$) δ ppm: 0.88 (t, 3H), 1.31 (m, 6H), 1.86 (m, 2H), 3.94 (s, 3H), 4.16 (t, 2H), 7.28 (s, 1H), 7.30 (s, 1H), 8.76 (s, 1H) (Kurnia et al., 2017; Rao and Gejji, 2016). All the IL FTIR spectra (Fig. S3) revealed characteristic peaks for RTILs (FTIR cm^{-1}): 3165 cm^{-1} (-CH stretching), 2960 cm^{-1} (-CH_2- asymmetric stretching), approximately 1572 cm^{-1} (-CH_2-N- and CH_3-N- symmetric / asymmetric stretching), 1466 cm^{-1} (CH_3-N-C-N- asymmetric stretching), 1350 m^{-1} (-SO_2- asymmetric stretching), 1176 cm^{-1} (-CF_3 asymmetric/symmetric stretching), 1052 cm^{-1} (S-N-S symmetric stretching), 791 cm^{-1} (-C-S- stretching), and 738 cm^{-1} (-C-F_3 symmetric bend).

The RTIL viscosity was measured using a spindle viscometer (Brookfield model DV-I prime, cone spindle CP-21) at 283.15 K . The increase of the cation alkyl chain length from C_2 to C_6 resulted in an increase in the viscosity, with measurements of ([E*mim*][TF_2N] = 51.5 mPa s, [Bmim][TF_2N] 106.5 mPa s, and [Hmim][TF_2N]=187.5 mPa s). RTIL thermogravimetric analysis (TGA) was performed using a TA model SDT Q600 instrument. The sample was heated from 25 to 700 °C under inert N_2 at a rate of 20 °C min^{-1}. The thermograms showed a thermal event

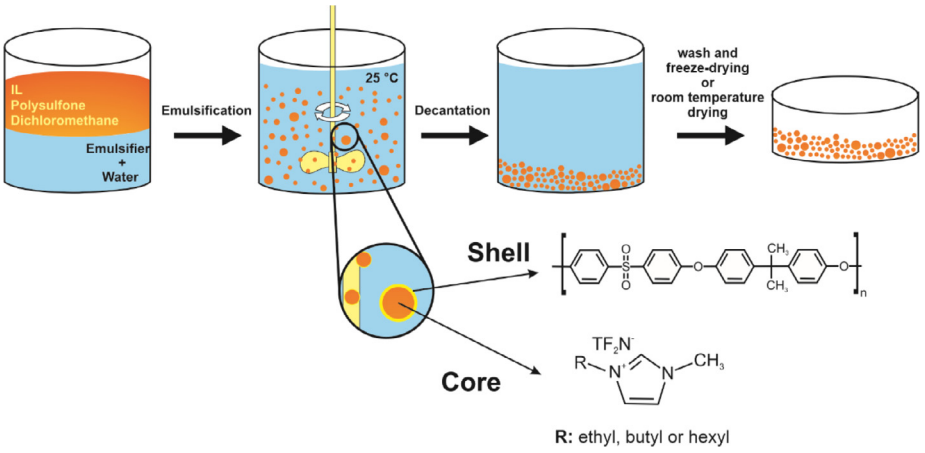

Fig. 1. Schematic representation of capsule fabrication.

for all RTILs (Fig. S4). The degradation onset temperature was similar (approximately 447 °C) for all RTILs. These results demonstrated the high thermal stability of the RTILs.

2.3. Microcapsule preparation

RTIL encapsulation (Fig. 1) was performed using experimental procedures adapted from the literature (Chen et al., 2012; Hao Li et al., 2016; Li et al., 2017). RTIL and PSF, in a weight ratio of 1.2:1.0, were dissolved in a minimal amount of dichloromethane. The mixture was then added to an aqueous solution containing 0.8 wt% (w/v) gelatin at 298.15 K. The mixture was emulsified for 300 s by stirring using Ultra-Turrax (with the speed ranging from 18,000 to 23,000 rpm). The capsules were collected by decantation, and the product was washed several times with distilled water. The dried encapsulated RTILs ([Bmim] [TF_2N] and [Hmim] [TF_2N]) were obtained by freeze-drying, while dried capsules of Emim TF_2N were obtained at a constant temperature of 298.15 K. The encapsulated RTIL was labeled as SXY-Vrpm, where X was the alkyl side chain length of the imidazolium cation, Y was an anion, and V was the stirring speed. For example, SBTF_2N-23 Krpm refers to the Bmim cation and TF_2N anion with a stirring speed of 23,000 rpm.

2.4. Characterization of microcapsules

The structures of samples were identified by FTIR. FTIR spectra were recorded on a Perkin-Elmer Spectrum 100 spectrometer in universal attenuated total reflectance (UATR) mode. The sample morphology was determined by field emission scanning electron microscopy (FESEM) using Inspect F50 equipment (FEI Instruments) in secondary electron mode and transmission electron microscopy (TEM) using a Tecnai G2 T20 FEI operating at 200 kV. Capsule sizes were measured using the ImageJ software. Differential scanning calorimetry (DSC) thermograms were obtained using a TA Instrument Q20 differential scanning calorimeter in the range from −90 °C to 250 °C at a heating rate of 10 °C/min under nitrogen for the polymer and encapsulated IL samples. TGA was performed using a TA Instruments SDTQ600 between 25 °C and 700 °C at a heating rate of 20 °C/min in a nitrogen atmosphere. RTIL loading in the shell (denoted as RTIL%) was obtained using the acetone extraction method(Hao Li et al., 2016; Ma et al., 2019). The experiments were performed in triplicates. The sample was dried for 4 h at 70 °C, weighed (w_1), fully ground in a mortar, and immersed in a solvent (acetone) for 48 h. The acetone completely dissolved the IL. Then, the polymer (PSF) was filtered, dried (4 h at 343.15 K), and weighed (w_2). The IL loading in the shell (RTIL%) was calculated using Eq. (1).

$$RTIL\ \% = \frac{w_1 - w_2}{w_1}\ x\ 100 \quad (1)$$

2.5. Sorption measurements

The pressure decay technique was used to determine the CO_2 sorption capacity. The dual-chamber gas sorption cell was similar to that reported by Koros et al. (Koros and Paul, 1976). The schematic CO_2 sorption apparatus is shown in Fig. S5. A detailed description of the sorption apparatus and measurement procedure can be found in our previous studies (Bernard et al., 2018, 2017; Fernández Rojas et al., 2017). The experiments were performed in triplicates. Approximately 1 g of sample was weighed and dried for 1 h at 343.15 K before the measurements. CO_2 sorption experiments were carried out at two different temperatures (298.15 K and 313.15 K) with pressures ranging from 1 to 10 bar.

The stability of the microcapsules was evaluated by seven CO_2 sorption/desorption cycles at 318.15 K and 4 bar with desorption following each cycle by heating at 343.15 K for 1 h.

3. Results and discussion

Encapsulated material properties are dependent on the morphology and capsule diameter (Podshivalov et al., 2013), and agitation speed greatly influences these properties (Podshivalov et al., 2013). Therefore, the stirring rate was varied (18,000 and 23,000 rpm) for capsule preparation. Fig. 2. shows the effect of stirring on the morphology of the encapsulated RTILs. The results corroborate that variations in the stirring rate influenced the RTIL capsule morphology. For a stirring rate of 23,000 rpm, [Bmim] [TF_2N] capsules with a smaller mean diameter and a more uniform distribution were obtained (Fig. 2b). The higher the agitation rate, the smaller the capsule size, resulting from a more potent stirring force in the mixing device(Podshivalov et al., 2013).

SBTF_2N-23 krpm (Fig. 2d) and SHTF_2N-23 krpm (Fig. 2f) showed average diameters ranging from 600 nm to 5 μm and 800 nm to 5.5 μm, respectively. It was challenging to obtain ideal capsules using 23,000 rpm to encapsulate [Emim] [TF_2N] (Fig. 2b) because the force of the agitation deformed the capsules. Using an 18,000 rpm stirring rate [Emim] [TF_2N], capsules with an average diameter ranging from 700 nm to 3 μm were formed (Fig. 2a).

The TEM images showed formation of spherically shaped capsules, as shown in Fig 3, with a polymer shell thickness of approximately 125 nm. In this work, the uniform spherically shaped capsules of SETF_2N-18 krpm, SBTF_2N-23 krpm, and SHTF_2N-23 krpm were selected for structural, thermal, and CO_2 sorption capacity evaluation.

The RTIL capsule FTIR spectrum (Fig. S6) showed characteristic peaks of PSF (Haiyan Hao Li et al., 2016; Li et al., 2017) at approximately 1586, 1505, and 1488 cm^{-1} (aromatic ring stretching), 1238 (*S=O* asymmetric stretching), and 1145 cm^{-1} (C–O-C). The spectrum also showed characteristic peaks of [$C_n$mim][TF_2N] IL(Ferreyra et al.,

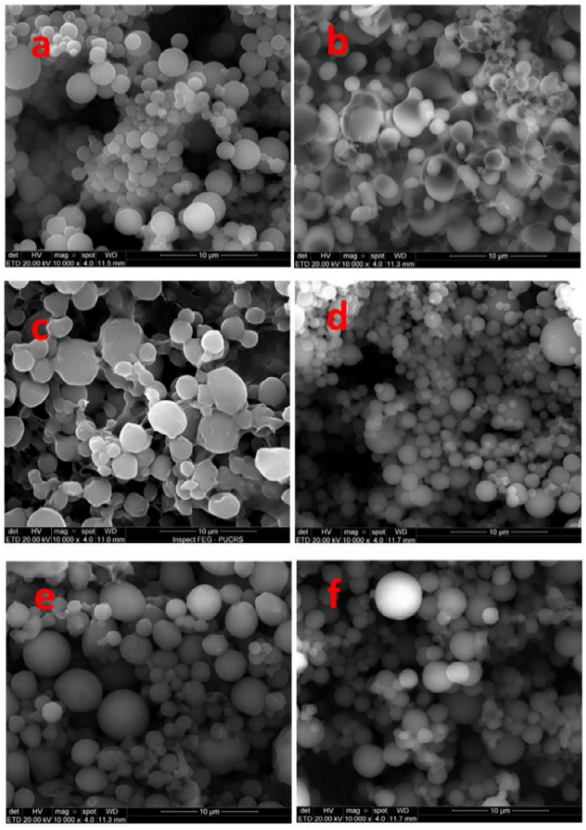

Fig. 2. Capsule FESEM images: a) $SETF_2N$-18 krpm, b) $SETF_2N$-23 krpm, c) $SBTF_2N$-18 krpm, d) $SBTF_2N$-23krpm, e) $SHTF_2N$-18 krpm and f) $SHTF_2N$-23 krpm.

Table 1
DSC data for PSF, RTIL, and RTIL capsules.

Sample	Tg (°C)	Tm (°C)	Tc (°C)
PSF	187.00	—	—
[Emim][Tf_2N]	—	−19.11	−48.73
[Bmim][Tf_2N]	—	−4.90	−27.20
[Hmim][Tf_2N]		−83.57	−58.45
$SETF_2N$-18 krpm	146.03	−17.75	−44.65
$SBTF_2N$-23 krpm	130.75	−3.14	−17.01
$SHTF_2N$-23 krpm	118.37	—	—

2012; Hao Hao Li et al., 2016; Noack et al., 2010; Zhang et al., 2018) at 3165 cm^{-1} (-CH stretching), at 2960 cm^{-1} (-CH_2- asymmetric stretching), at approximately 1586 cm^{-1} (-CH_2–N- and CH_3–N- symmetric / asymmetric stretching), at approximately 1466 cm^{-1} (CH_3–N-C–N- asymmetric stretching), at 1350 cm^{-1} (-SO_2- asymmetric stretching), at 1176 cm^{-1} (-CF_3 asymmetric/symmetric stretching), at 1052 cm^{-1} (S-N-S symmetric stretching), at 791 cm^{-1} (-C-S- stretching), and at 738 cm^{-1} (-C-F_3 symmetric bending). Therefore, the FTIR results confirm RTIL encapsulation within the polysulfone shell.

The RTIL–polymer interactions were studied by DSC analysis (Fig. S7 and Table 1). The DSC curves for the RTIL capsule were compared with those of the non-encapsulated IL and bare PSF. DSC curves of RTIL and capsules containing [Emim][TF_2N] and [Bmim][TF_2N] RTIL showed endothermic and exothermic peaks corresponding to the melting (Tm) and crystallization (Tc) of RTIL, respectively. The solid-liquid phase transition behavior of some RTILs is somewhat complicated (Huddleston et al., 2001). The existence of these peaks may result from the symmetry and planarity of the compounds (Min et al., 2006). Bonhôte et al. showed that the correlation between the RTIL chemical composition and melting point is difficult to determine (Bonhôte et al., 1996). The Tm and

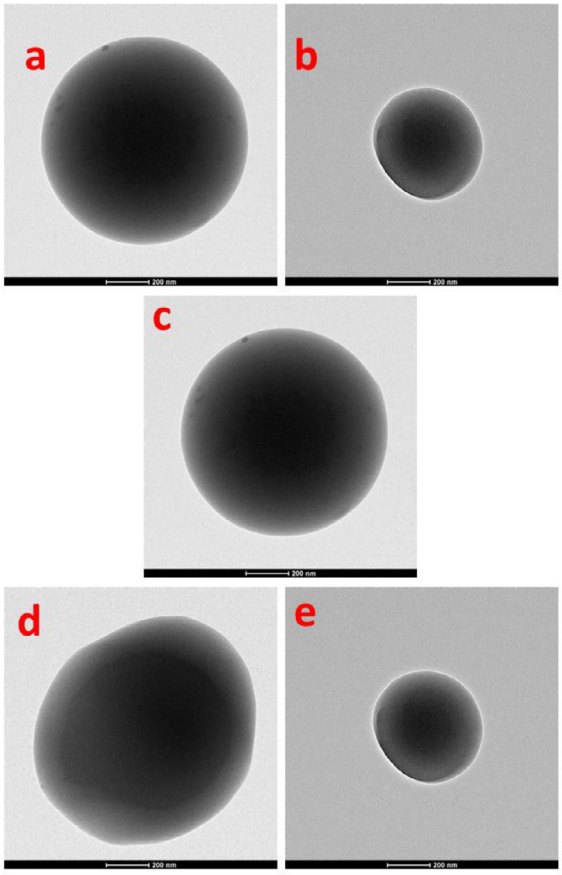

Fig. 3. Capsule TEM images: a) SETF2N-18 krpm, b) SETF2N-23 krpm, c) SBTF2N-23 krpm, b) SHTF2N-18 krpm, and e) SHTF2N-23 krpm,.

Tc values of capsules tended to be higher when compared to the non-encapsulated RTIL, possibly due to the amorphous shell (Table 1), as encapsulated drugs exhibit similar behaviors (Luan, 2011). A decrease in the glass transition temperature (Tg) of all encapsulated RTILs was also observed compared to the bare PSF (Fig. S7 and Table 1). Furthermore, it was noted that there was a trend for the Tg to decrease with an increase in the encapsulated IL content and IL viscosity (Fig. S7 and Table 1). This observation is consistent with the IL polymer composite described in the literature (Mohshim et al., 2016; Shalu et al., 2015). The increase in IL viscosity leads to enhancements in the polymer amorphicity, resulting in decreased Tg values (Mohshim et al., 2016). Thus, RTILs inserted into polymeric structures acted as plasticizers, improving chain flexibility, facilitating motion, and reducing polymer Tg (Gao et al., 2013; Mohshim et al., 2016; Shalu et al., 2015).

The thermal stability of PSF and the encapsulated RTIL was investigated by TGA (Fig. S8). The degradation onset temperature of the PSF was 525 °C. The RTIL capsule degradation temperature was lower than that of PSF, indicating successful RTIL encapsulation within the polysulfone shell. TGA results also showed that RTIL capsules could be used at temperatures below 436 °C (T_{onset}). The PSF residual weight was 32.5 wt% at 700 °C, which was probably linked to the formation of thermally stable carbonaceous materials (Haiyan Hao Li et al., 2016; Li et al., 2017). Overall, encapsulated RTILs had a lower residual weight than PSF. The residual weights found for [Emim][TF_2N], [Bmim][TF_2N] and [Hmim][TF_2N] were 14.9%, 11.7% and 8.0 wt%, respectively. The residual weight reduction was in agreement with the encapsulation capacity trend shown in Fig. S8. Fig. 4. Presents the encapsulation capacity (RTIL%) obtained using the acetone extraction method.

The encapsulation capacity tended to increment with the increase of cation alkyl chain length from C_2 to C_6, as seen in Fig. 4, possibly due to

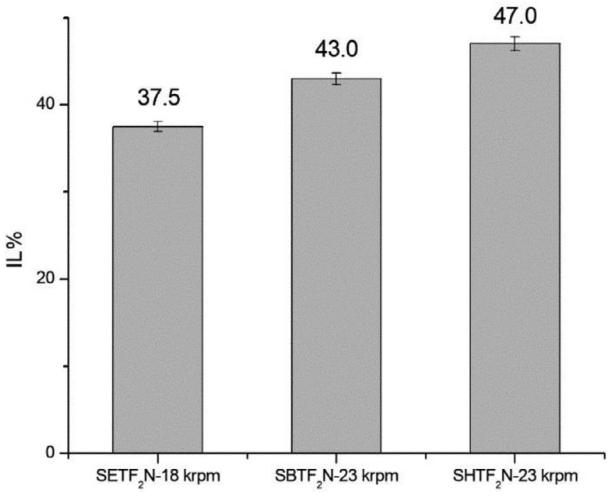

Fig 4. Capsule encapsulation capacity.

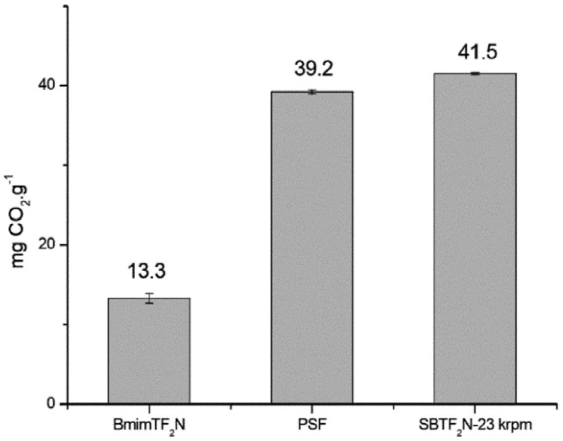

Fig. 5. CO_2 sorption values of sorbent materials at 4 bar and 318.15 K.

increases in RTIL viscosity ([E*mim*][TF_2N] = 51.5 mPa s; [Bmim TF_2N] =106.5 mPa s; Hmim TF_2N] =187.5 mPa).

Fig. 5 presents encapsulated [Bmim][TF_2N], non - encapsulated IL and PSF CO_2 sorption capacity at 4 bar and 318.15 K. PSF, specifically, has an adsorptive capacity (39.2 mgCO_2/*g* ±0.25), most likely due to the interaction between the CO_2 molecule and the polar groups (Gabrienko et al., 2016; Tomasko et al., 2003). The solubility tended to increase with the encapsulation of RTIL within the polymeric shell. Encapsulated [Bmim][TF_2N] (41.5 mgCO_2/*g* ± 0.12) exhibited high CO_2 capture capacity when compared to non - encapsulated RTIL (13.3 mg CO_2/*g* ± 0.6). The CO_2 sorption capacity of RTILs results from intermolecular interactions between the RTILs and CO_2. Furthermore, the molecular structure of RTILs creates a larger free volume to accommodate more CO_2 molecules (Palgunadi et al., 2009). However, encapsulated RTILs may increase the surface area and solvent CO_2 sorption rate (Aines et al., 2013; Stolaroff et al., 2016; Vericella et al., 2015). Solvent encapsulation may promote an increase in CO_2 sorption rate due to enhancement in mass transfer rate. Increasing surface area leads to a faster CO_2 diffusion through the polymer shell facilitating controlled CO_2 sorption and release over repeated cycles(Vericella et al., 2015). These results suggest a synergistic effect between [Bmim][TF_2N] RTIL and PSF, increasing CO_2 sorption in the encapsulated RTIL. This behavior was similar to that reported by Kaviani et al. 2018(Kaviani et al., 2018b).

The cost and viscosity of RTILs are the main drawbacks of using these green solvents for CO_2 capture, but RTIL microencapsulation can address this challenge (Stolaroff et al., 2016). Moreover, RTIL encapsulation may increase both the surface area and sorbent CO_2 sorption rate (Aines et al., 2013; Stolaroff et al., 2016). Fig. 6 presents the CO_2 sorption kinetics of encapsulated [Bmim][TF_2N] compared to that of the bare RTIL.

The encapsulation of [Bmim][TF_2N] dramatically increased the rate of CO_2 sorption. The CO_2 sorption rate of bare [Bmim][TF_2N] was substantially lower (saturation time around 44 min) than that of encapsulated [Bmim][TF_2N] (saturation time around 5 min), most likely because of the high viscosity of [Bmim][TF_2N], resulting in low CO_2 diffusion coefficient values and high resistance to mass transfer(Moya et al., 2016).

The CO_2 sorption capacity of the microcapsules was investigated at pressures ranging from 1 to 10 bar at two temperatures (see Figs. 7 and 8). CO_2 sorption increased as the temperature decreased and pressure increased for all microcapsules, indicating typical physical solvent behavior (Borhani and Wang, 2019; Yu et al., 2012). Experimental and simulation studies have shown that an increase in the alkyl side chain of the imidazolium cation can result in increased CO_2 sorption owing to an increase in the RTIL free volume used to capture CO_2 molecules (Condemarin and Scovazzo, 2009; Ferguson and Scovazzo, 2007; Hou and Baltus, 2007; Sarmad et al., 2017; Shannon et al., 2012; Shiflett and Yokozeki, 2005). However, an opposite trend is observed for the microcapsules, as shown in Figs. 7 and 8, CO_2 sorption capacity tended to increase with the reduction of cation alkyl chain length from C_6 to C_2, possibly due to a reduction in the encapsulation capacity and RTIL viscosity ([Hmim TF_2N] =187.5 mPa s; [Bmim TF_2N] =106.5 mPa s; [Emim][TF_2N] = 51.5 mPa s). High RTIL viscosity can

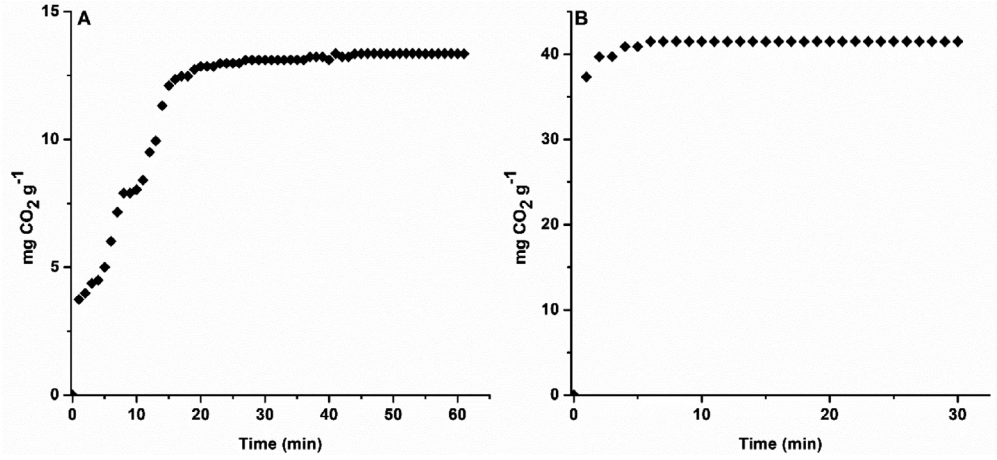

Fig. 6. CO_2 sorption kinetics (a) non-encapsulated [Bmim][TF_2N] (b) encapsulated [Bmim][TF_2N] (SBTF$_2$N-23 krpm). CO_2 sorption values at 4 bar and 318.15 K.

Table 2
Comparison of $SETF_2N$-18 krpm with different encapsulated ILs in terms of CO_2 sorption capacity.

Shell	Ionic Liquid (IL)	Experimental Condition (bar - Kelvin)	CO_2 Loading		Ref.
			mg g^{-1}	mmol g^{-1}	
PSF	[Emim][TF_2N] IL	10 – 298.15	62.7	1.42	This work
PSF	[Emim][TF_2N] IL	1 – 298.15	39.5	0.90	This work
PVDF-HFP	[Emim][TF_2N] IL	10 - 296.15	–	~1.20	(Kaviani et al., 2018a)
C_{Cap} support	[Bmim][Gly] IL	1–303	38	–	(Santiago et al., 2018)
C_{Cap} support	[Bmim][PRO] IL	1–303	31	–	(Santiago et al., 2018)
C_{Cap} support	[Bmim][MET] IL	1–303	20	–	(Santiago et al., 2018)

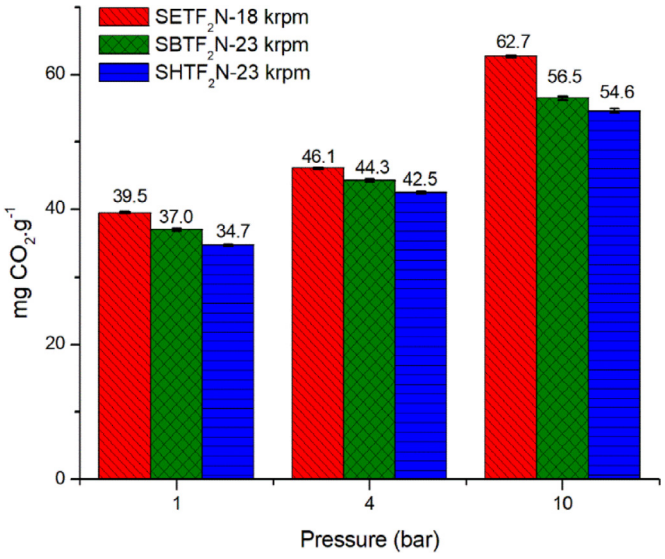

Fig. 7. Microcapsules CO_2 sorption at 298.15 K and different pressures.

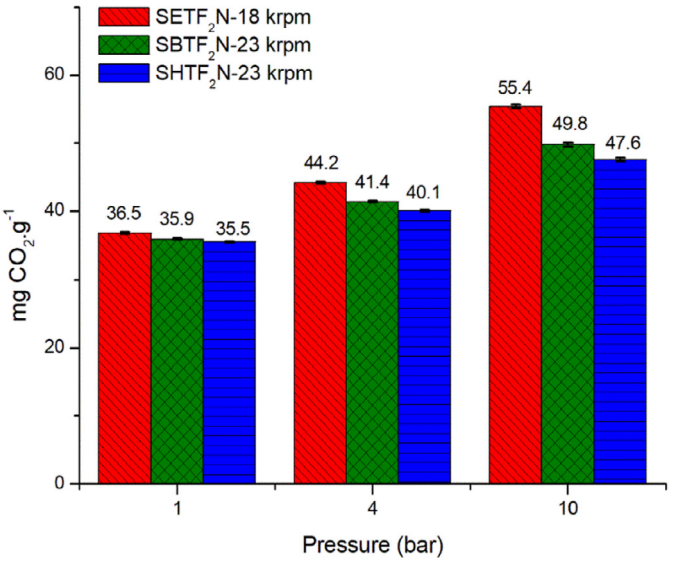

Fig. 8. Microcapsules CO_2 sorption at 318.15 K and different pressures.

result in a low CO_2 diffusion coefficient and high resistance to mass transfer (Moya et al., 2016). In all tests, sample $SETF_2N$-18 krpm was found to have the highest CO_2 sorption value. This sample presented the lowest encapsulation capacity (37.5% ± 0.6) compared to the other samples, indicating that encapsulation of a lower [Emim] [TF_2N] concentration resulted in a higher CO_2 sorption capacity.

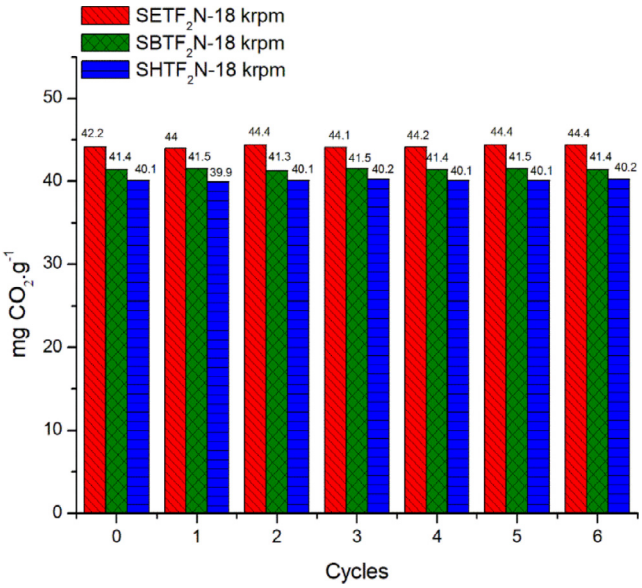

Fig. 9. Microcapsules CO_2 sorption/desorption cycles. Conditions: CO_2 sorption at 4 bar and 318.15 K.; desorption: 343.15 K for 1 h.

The CO_2 sorption capacities of the $SETF_2N$-18 krpm capsules were compared with those of the encapsulated RTILs reported in the literature (Table 2). At comparable temperatures and pressures, performance data showed the CO_2 sorption capacity for encapsulated [Emim][TF_2N] described in this work was higher than those reported by other authors.

Sorption/desorption cycles were performed to evaluate the stability of the microcapsules during the CO_2 capture processes. The CO_2 sorption capacity of all microcapsules was reversible for seven consecutive cycles (Fig. 9).

The CO_2 sorption tests were performed at 4 bar and 318.15 K. After each step, CO_2 desorption was carried out at 343.15 K for 1 h. Fig. 9 presents the results of seven consecutive tests. All microcapsules could be regenerated under mild conditions, suggesting that the encapsulation of RTILs in PSF has good potential for use as a CO_2 capture sorbent.

4. Conclusion

The effect of the alkyl side chain length of imidazolium cations (C_2, C_4, and C_6) containing TF_2N anions on the morphology, thermal stability, encapsulation capacity (IL%), and CO_2 sorption capacity of the encapsulated RTILs was investigated. The results showed that the agitation rate influenced the capsule morphology and diameter. The CO_2 sorption capacity of the encapsulated RTIL was superior to that of bare RTIL and PSF. The high performance of the RTIL capsules was likely related to the attraction between CO_2 molecules and the encapsulated RTIL. Encapsulated [Emim][TF_2N] showed a higher CO_2 sorption capacity than the encapsulated RTILs reported in the literature. The CO_2 sorption capacity

tended to increase with a reduction in the cation alkyl chain length. All the encapsulated RTILs showed high stability and reuse capacity in the CO_2 capture processes. The highest CO_2 sorption capacity was observed for sample SETF_2N-18 krpm. However, this microcapsule presented the lowest encapsulation capacity (37.5% ± 0.6) compared to other RTIL microcapsules.

Declaration of Competing Interest

The authors declare that they have no known competing financial interests or personal relationships that could have appeared to influence the work reported in this paper.

Acknowledgments

The authors acknowledge support from Shell Brazil and the strategic importance of the support provided by the ANP (Brazil's National Oil, Natural Gas, and Biofuels Agency) through the R&D levy regulation. Sandra Einloft thanks CNPq for his research scholarship. Rafael Duczinski and Barbara B. Polesso thank CAPES for his Ph.D. scholarship. This study was financed in part by the Coordenação de Aperfeiçoamento de Pessoal de Nível Superior – Brasil (CAPES) – Finance Code 001.

Supplementary materials

Supplementary material associated with this article can be found, in the online version, at doi:10.1016/j.envc.2021.100109.

Reference

Ağralı, S., Üçtuğ, F.G., Türkmen, B.A., 2018. An optimization model for carbon capture & storage/utilization vs. carbon trading: a case study of fossil-fired power plants in Turkey. J. Environ. Manag. 215, 305–315. doi:10.1016/j.jenvman.2018.03.054.

Aines, R.D., Spaddaccini, C.M., Duoss, E.B., Stolaroff, J.K., Vericella, J., Lewis, J.A., Farthing, G., 2013. Encapsulated solvents for carbon dioxide capture. Energy Procedia 37, 219–224. 10.1016/j.egypro.2013.05.105

Aki, S.N.V.K., Mellein, B.R., Saurer, E.M., Brennecke, J.F., 2004. High-pressure phase behavior of carbon dioxide with imidazolium-based ionic liquids. J. Phys. Chem. B 108, 20355–20365 10.1021/jp046895+.

Anthony, J.L., Anderson, J.L., Maginn, E.J., Brennecke, J.F., 2005. Anion effects on gas solubility in ionic liquids. J. Phys. Chem. B 109, 6366–6374. doi:10.1021/jp046404l.

Anthony, J.L., Maginn, E.J., Brennecke, J.F., 2002a. Solubilities and thermodynamic properties of gases in the ionic liquid 1- n -Butyl-3-methylimidazolium Hexafluorophosphate. J. Phys. Chem. B 106, 7315–7320. doi:10.1021/jp020631a.

Anthony, J.L., Maginn, E.J., Brennecke, J.F., 2002b. Solubilities and thermodynamic properties of gases in the ionic liquid 1- n -Butyl-3-methylimidazolium Hexafluorophosphate. J. Phys. Chem. B 106, 7315–7320. doi:10.1021/jp020631a.

Anwar, M.N., Fayyaz, A., Sohail, N.F., Khokhar, M.F., Baqar, M., Khan, W.D., Rasool, K., Rehan, M., Nizami, A.S., 2018. CO_2 capture and storage: a way forward for sustainable environment. J. Environ. Manag. 226, 131–144. doi:10.1016/j.jenvman.2018.08.009.

Bai, L., Shang, D., Li, M., Dai, Z., Deng, L., Zhang, X., 2017. CO_2 absorption with ionic liquids at elevated temperatures. J. Energy Chem. 26, 1001–1006. doi:10.1016/j.jechem.2017.07.009.

Bernard, F.L., dos Santos, L.M., Schwab, M.B., Polesso, B.B., do Nascimento, J.F., Einloft, S., 2019a. Polyurethane-based poly (ionic liquid)s for CO_2 removal from natural gas. J. Appl. Polym. Sci. 47536. doi:10.1002/app.47536.

Bernard, F.L., Duczinski, R.B., Rojas, M.F., Fialho, M.C.C., Carreño, L.Á., Chaban, V.V., Vecchia, F.D., Einloft, S., 2018. Cellulose based poly(ionic liquids): tuning cation-anion interaction to improve carbon dioxide sorption. Fuel 211, 76–86. doi:10.1016/j.fuel.2017.09.057.

Bernard, F.L., Polesso, B.B., Cobalchini, F.W., Chaban, V.V., do Nascimento, J.F., Dalla Vecchia, F., Einloft, S., 2017. Hybrid Alkoxysilane-functionalized urethane-imide-based poly(ionic liquids) as a new platform for carbon dioxide capture. Energy Fuels 31, 9840–9849. doi:10.1021/acs.energyfuels.7b02027.

Bernard, F.L., Polesso, B.B., Cobalchini, F.W., Donato, A.J., Seferin, M., Ligabue, R., Chaban, V.V., do Nascimento, J.F., Dalla Vecchia, F., Einloft, S., 2016. CO2 capture: tuning cation-anion interaction in urethane based poly(ionic liquids). Polymer 102, 199–208. doi:10.1016/j.polymer.2016.08.095.

Bernard, F.L., Rodrigues, D.M., Polesso, B.B., Chaban, V.V., Serefin, M., Dalla Vecchia, F., Einloft, S., 2019b. Development of inexpensive cellulose-based sorbents for carbon dioxide. Brazilian J. Chem. Eng. 36, 511–521. doi:10.1590/0104-6632.20190361s20170182.

Bernard, Franciele Longaray, Santos, L.M.dos, Cobalchina, F.W., Schwab, M.B., Einloft, S., 2019. Polyurethane/poly (Ionic liquids) cellulosic composites and their evaluation for separation of CO_2 from natural gas. Mater. Res. 22. doi:10.1590/1980-5373-mr-2018-0827.

Blanchard, L.A., Gu, Z., Brennecke, J.F., 2001. High-Pressure phase behavior of ionic liquid /CO2 systems. J. Phys. Chem. B 105, 2437–2444. doi:10.1021/jp003309d.

Bonhôte, P., Dias, A.-P., Papageorgiou, N., Kalyanasundaram, K., Grätzel, M., 1996. Hydrophobic, highly conductive ambient-temperature molten salts †. Inorg. Chem. 35, 1168–1178. doi:10.1021/ic951325x.

Borhani, T.N.G., Azarpour, A., Akbari, V., Wan Alwi, S.R., Manan, Z.A., 2015. CO2 capture with potassium carbonate solutions: a state-of-the-art review. Int. J. Greenh. Gas Control 41, 142–162. doi:10.1016/j.ijggc.2015.06.026.

Brennecke, J.F., Gurkan, B.E., 2010. Ionic liquids for CO_2 capture and emission reduction. J. Phys. Chem. Lett. 1, 3459–3464. doi:10.1021/jz1014828.

Cadena, C., Anthony, J.L., Shah, J.K., Morrow, T.I., Brennecke, J.F., Maginn, E.J., 2004. Why is CO_2 so soluble in imidazolium-based ionic liquids? J. Am. Chem. Soc. 126, 5300–5308. doi:10.1021/ja039615x.

Camper, D., Scovazzo, P., Koval, C., Noble, R., 2004. Gas solubilities in room-temperature ionic liquids. Ind. Eng. Chem. Res. 43, 3049–3054. doi:10.1021/ie034097k.

Chen, D.X., OuYang, X.K., Wang, Y.G., Yang, L.Y., Yu, D., 2012. Polysulfone microcapsules containing ionic liquid. Adv. Mater. Res 554–556, 273–276. doi:10.4028/www.scientific.net/AMR.554-556.273.

Condemarin, R., Scovazzo, P., 2009. Gas permeabilities, solubilities, diffusivities, and diffusivity correlations for ammonium-based room temperature ionic liquids with comparison to imidazolium and phosphonium RTIL data. Chem. Eng. J. 147, 51–57. doi:10.1016/j.cej.2008.11.015.

Duczinski, R., Polesso, B.B., Bernard, F.L., Ferrari, H.Z., Almeida, P.L., Corvo, M.C., Cabrita, E.J., Menezes, S., Einloft, S., 2020. Enhancement of CO_2/N_2 selectivity and CO_2 uptake by tuning concentration and chemical structure of imidazolium-based ILs immobilized in mesoporous silica. J. Environ. Chem. Eng. 8, 103740. doi:10.1016/j.jece.2020.103740.

Einloft, S., Bernard, F.L., 2020. Encapsulated liquid sorbents for CO_2 capture. In: Advances in Carbon Capture.. Elsevier, pp. 125–150. doi:10.1016/B978-0-12-819657-1.00006-2.

Farahipour, R., Karunanithi, A.T., 2014. Life cycle environmental implications of CO_2 capture and sequestration with ionic liquid 1-Butyl-3-methylimidazolium acetate. ACS Sustain. Chem. Eng. 2, 2495–2500. doi:10.1021/sc400274b.

Ferguson, L., Scovazzo, P., 2007. Solubility, diffusivity, and permeability of gases in phosphonium-based room temperature ionic liquids: data and correlations. Ind. Eng. Chem. Res. 46, 1369–1374. doi:10.1021/ie0610905.

Fernández Rojas, M., Pacheco Miranda, L., Martinez Ramirez, A., Pradilla Quintero, K., Bernard, F., Einloft, S., Carreño Díaz, L.A., 2017. New biocomposites based on castor oil polyurethane foams and ionic liquids for CO_2 capture. Fluid Phase Equilib 452, 103–112. doi:10.1016/j.fluid.2017.08.026.

Ferreyra, D.D., Correa, N.M., Silber, J.J., Falcone, R.D., 2012. The effect of different interfaces and confinement on the structure of the ionic liquid 1-butyl-3-methylimidazolium bis(trifluoromethylsulfonyl)imide entrapped in cationic and anionic reverse micelles. Phys. Chem. Chem. Phys. 14, 3460. doi:10.1039/c2cp23481e.

Freire, M.G., Carvalho, P.J., Gardas, R.L., Marrucho, I.M., Santos, L.M.N.B.F., Coutinho, J.A.P., 2008. Mutual solubilities of water and the [Cnmim][Tf2N] hydrophobic ionic liquids. J. Phys. Chem. B 112, 1604–1610. doi:10.1021/jp7097203.

Gabrienko, A.A., Ewing, A.V., Chibiryaev, A.M., Agafontsev, A.M., Dubkov, K.A., Kazarian, S.G., 2016. New insights into the mechanism of interaction between CO $_2$ and polymers from thermodynamic parameters obtained by in situ ATR-FTIR spectroscopy. Phys. Chem. Chem. Phys. 18, 6465–6475. doi:10.1039/C5CP06431G.

Gao, R., Zhang, M., Wang, S.-W., Moore, R.B., Colby, R.H., Long, T.E., 2013. Polyurethanes containing an imidazolium diol-based ionic-liquid chain extender for incorporation of ionic-liquid electrolytes. Macromol. Chem. Phys. 214, 1027–1036. doi:10.1002/macp.201200688.

Gudoshava, M., Misiani, H.O., Segele, Z.T., Jain, S., Ouma, J.O., Otieno, G., Anyah, R., Indasi, V.S., Endris, H.S., Osima, S., Lennard, C., Zaroug, M., Mwangi, E., Nimusiima, A., Kondowe, A., Ogwang, B., Artan, G., Atheru, Z., 2020. Projected effects of 1.5 °C and 2 °C global warming levels on the intra-seasonal rainfall characteristics over the Greater Horn of Africa. Environ. Res. Lett. 15, 034037. doi:10.1088/1748-9326/ab6b33.

Hanioka, S., Maruyama, T., Sotani, T., Teramoto, M., Matsuyama, H., Nakashima, K., Hanaki, M., Kubota, F., Goto, M., 2008. CO_2 separation facilitated by task-specific ionic liquids using a supported liquid membrane. J. Memb. Sci. 314, 1–4. doi:10.1016/j.memsci.2008.01.029.

Hasib-ur-Rahman, M., Siaj, M., Larachi, F., 2010. Ionic liquids for CO_2 capture-development and progress. Chem. Eng. Process. Process Intensif. 49, 313–322. doi:10.1016/j.cep.2010.03.008.

Hernández, M.F.A., Rojas, M.F., Bernard, F., Einloft, S., Diaz, L.A.C., 2020. Mixtures of cellulose fibers from pineapple leaves, ionic liquid, and alkanolamines for CO_2 capture. Fibers Polym 21, 2861–2872. doi:10.1007/s12221-020-0094-3.

Hou, Y., Baltus, R.E., 2007. Experimental measurement of the solubility and diffusivity of CO_2 in room-temperature ionic liquids using a transient thin-liquid-film method. Ind. Eng. Chem. Res. 46, 8166–8175. doi:10.1021/ie070501u.

Huddleston, J.G., Visser, A.E., Reichert, W.M., Willauer, H.D., Broker, G.A., Rogers, R.D., 2001. Characterization and comparison of hydrophilic and hydrophobic room temperature ionic liquids incorporating the imidazolium cation. Green Chem 3, 156–164. doi:10.1039/b103275p.

Jairton, D., Consorti, C.S., Suarez, P.A.Z., de, Souza, R.F., 2002. Preparation of 1-butyl-3-methyl imidazolium-based room temperature ionic liquids. Org. Synth. 79, 236. doi:10.15227/orgsyn.079.0236.

Kaviani, S., Kolahchyan, S., Hickenbottom, K.L., Lopez, A.M., Nejati, S., 2018a. Enhanced solubility of carbon dioxide for encapsulated ionic liquids in polymeric materials. Chem. Eng. J. 354, 753–757. doi:10.1016/j.cej.2018.08.086.

Kaviani, S., Kolahchyan, S., Hickenbottom, K.L., Lopez, A.M., Nejati, S., 2018b. Enhanced solubility of carbon dioxide for encapsulated ionic liquids in polymeric materials. Chem. Eng. J. 354, 753–757. doi:10.1016/j.cej.2018.08.086.

Ketzel, João Marcelo, Igleisias, Rodrigo, Einloft, S., 2015. Reducing greenhouse gas emissions with CO_2 capture and geological storage. In: Chen, Wei-Yin, Toshio Suzuki, M.L. (Eds.), Handbook of Climate Change Mitigation and Adaptation, pp. 1–40. doi:10.1007/978-1-4614-6431-0_37-2.

Koros, W.J., Paul, D.R., 1976. Design considerations for measurement of gas sorption in polymers by pressure decay. J. Polym. Sci. Polym. Phys. Ed. 14, 1903–1907. doi:10.1002/pol.1976.180141014.

Kurnia, K.A., Sintra, T.E., Danten, Y., Cabaço, M.I., Besnard, M., Coutinho, J.A.P., 2017. A simple method for preparation of a novel hydrophobic ionic liquid with a per-fluoro-tert-butoxide anion. New J. Chem. 41, 47–50. doi:10.1039/C6NJ02575G.

Li, H., Cui, Y., Wang, H., Zhu, Y., Wang, B., 2017. Preparation and application of polysulfone microcapsules containing tung oil in self-healing and self-lubricating epoxy coating. Colloids Surf. A Physicochem. Eng. Asp. 518, 181–187. doi:10.1016/j.colsurfa.2017.01.046.

Li, Hao, Tuo, L., Yang, K., Jeong, H.-.K., Dai, Y., He, G., Zhao, W., 2016a. Simultaneous enhancement of mechanical properties and CO_2 selectivity of ZIF-8 mixed matrix membranes: interfacial toughening effect of ionic liquid. J. Memb. Sci. 511, 130–142. doi:10.1016/j.memsci.2016.03.050.

Luan, 2011. Ibuprofen-loaded poly(lactic-co-glycolic acid) films for controlled drug release. Int. J. Nanomedicine 659. doi:10.2147/IJN.S17011.

Ma, Y., Li, Z., Wang, H., Li, H., 2019. Synthesis and optimization of polyurethane microcapsules containing [BMIm]PF6 ionic liquid lubricant. J. Colloid Interface Sci. 534, 469–479. doi:10.1016/j.jcis.2018.09.059.

McGurk, S.J., Martín, C.F., Brandani, S., Sweatman, M.B., Fan, X., 2017. Microwave swing regeneration of aqueous monoethanolamine for post-combustion CO2 capture. Appl. Energy 192, 126–133. doi:10.1016/j.apenergy.2017.02.012.

Min, G.H., Yim, T., Hyun, Y.L., Dal, H.H., Lee, E., Mun, J., Oh, S.M., Young, G.K., 2006. Synthesis and properties of ionic liquids: imidazolium tetrafluoroborates with unsaturated side chains. Bull. Korean Chem. Soc. 27, 847–852. doi:10.5012/bkcs.2006.27.6.847.

Mohshim, D.F., Mukhtar, H., Man, Z., 2016. Composite blending of ionic liquid-poly(ether sulfone) polymeric membranes: green materials with potential for carbon dioxide/methane separation. J. Appl. Polym. Sci. 133. doi:10.1002/app.43999.

Moya, C., Alonso-Morales, N., Gilarranz, M.A., Rodriguez, J.J., Palomar, J., 2016. Encapsulated ionic liquids for CO_2 capture: using 1-butyl-methylimidazolium acetate for quick and reversible CO_2 chemical absorption. ChemPhysChem 17, 3891–3899. doi:10.1002/cphc.201600977.

Nie, L., Mu, Y., Jin, J., Chen, J., Mi, J., 2018. Recent developments and consideration issues in solid adsorbents for CO_2 capture from flue gas. Chin, J. Chem. Eng. 26, 2303–2317. doi:10.1016/j.cjche.2018.07.012.

Noack, K., Schulz, P.S., Paape, N., Kiefer, J., Wasserscheid, P., Leipertz, A., 2010. The role of the C_2 position in interionic interactions of imidazolium based ionic liquids: a vibrational and NMR spectroscopic study. Phys. Chem. Chem. Phys. 12, 14153. doi:10.1039/c0cp00486c.

Olajire, A.A., 2010. CO2 capture and separation technologies for end-of-pipe applications - A review. Energy 35, 2610–2628. doi:10.1016/j.energy.2010.02.030.

Palgunadi, J., Kang, J.E., Cheong, M., Kim, H., Lee, H., Kim, H.S., 2009. Fluorine-free imidazolium-based ionic liquids with a phosphorous-containing anion as potential CO_2 absorbents. Bull. Korean Chem. Soc. 30, 1749–1754. doi:10.5012/bkcs.2009.30.8.1749.

Podshivalov, A.V., Bronnikov, S., Zuev, V.V., Jiamrungraksa, T., Charuchinda, S., 2013. Synthesis and characterization of polyurethane–urea microcapsules containing galangal essential oil: statistical analysis of encapsulation. J. Microencapsul. 30, 198–203. doi:10.3109/02652048.2012.735261.

Privalova, E.I., Mäki-Arvela, P., Murzin, D.Y., Mikkhola, J.P., 2012. Capturing CO_2 : conventional versus ionic-liquid based technologies. Russ. Chem. Rev. 81, 435–457. doi:10.1070/RC2012v081n05ABEH004288.

Rao, S.S., Gejji, S.P., 2016. Electronic structure, NMR, spin–spin coupling, and noncovalent interactions in aromatic amino acid based ionic liquids. J. Phys. Chem. A 120, 5665–5684. doi:10.1021/acs.jpca.6b03985.

Roefs, P., Moretti, M., Welkenhuysen, K., Piessens, K., Compernolle, T., 2019. CO_2 -enhanced oil recovery andCO_2 capture and storage: an environmental economic trade-off analysis. J. Environ. Manag. 239, 167–177. doi:10.1016/j.jenvman.2019.03.007.

Sadeghpour, M., Yusoff, R., Aroua, M.K., 2016. Polymeric ionic liquids (PILs) for CO_2 capture. Rev. Chem. Eng. 0. doi:10.1515/revce-2015-0070.

Santiago, R., Lemus, J., Moya, C., Moreno, D., Alonso-Morales, N., Palomar, J., 2018. Encapsulated ionic liquids to enable the practical application of amino acid-based ionic liquids in CO_2 capture. ACS Sustain. Chem. Eng. 6, 14178–14187. doi:10.1021/acssuschemeng.8b02797.

Sarmad, S., Mikkola, J.-.P., Ji, X., 2017. Carbon dioxide capture with ionic liquids and deep eutectic solvents: a new generation of sorbents. ChemSusChem 10, 324–352. doi:10.1002/cssc.201600987.

Shalu, Chaurasia, Singh, S.K., Chandra, S., R.K., 2015. Electrical, mechanical, structural, and thermal behaviors of polymeric gel electrolyte membranes of poly(vinylidene fluoride- co -hexafluoropropylene) with the ionic liquid 1-butyl-3-methylimidazolium tetrafluoroborate plus lithium tetrafluoroborate. J. Appl. Polym. Sci. 132. doi:10.1002/app.41456, n/a-n/a.

Shannon, M.S., Tedstone, J.M., Danielsen, S.P.O., Hindman, M.S., Irvin, A.C., Bara, J.E., 2012. Free volume as the basis of gas solubility and selectivity in imidazolium-based ionic liquids. Ind. Eng. Chem. Res. 51, 5565–5576. doi:10.1021/ie202916e.

Shiflett, M.B., Yokozeki, A., 2005. Solubilities and diffusivities of carbon dioxide in ionic liquids: [bmim][PF 6] and [bmim][BF 4]. Ind. Eng. Chem. Res. 44, 4453–4464. doi:10.1021/ie058003d.

Shiogama, H., Hirata, R., Hasegawa, T., Fujimori, S., Ishizaki, N.N., Chatani, S., Watanabe, M., Mitchell, D., Lo, Y.T.E., 2020. Historical and future anthropogenic warming effects on droughts, fires and fire emissions of CO_2 and PM2.5 in equatorial Asia when 2015-like El Niño events occur. Earth Syst. Dyn. 11, 435–445. doi:10.5194/esd-11-435-2020.

Stolaroff, J.K., Ye, C., Oakdale, J.S., Baker, S.E., Smith, W.L., Nguyen, D.T., Spadaccini, C.M., Aines, R.D., 2016. Microencapsulation of advanced solvents for carbon capture. Faraday Discuss 192, 271–281. doi:10.1039/C6FD00049E.

Tang, J., Sun, W., Tang, H., Radosz, M., Shen, Y., 2005. Enhanced CO_2 absorption of poly(ionic liquid)s. Macromolecules 38, 2037–2039. doi:10.1021/ma047574z.

Tomasko, D.L., Li, H., Liu, D., Han, X., Wingert, M.J., Lee, L.J., Koelling, K.W., 2003. A review of CO_2 applications in the processing of polymers. Ind. Eng. Chem. Res. 42, 6431–6456. doi:10.1021/ie030199z.

Vericella, J.J., Baker, S.E., Stolaroff, J.K., Duoss, E.B., Hardin, J.O., Lewicki, J., Glogowski, E., Floyd, W.C., Valdez, C.A., Smith, W.L., Satcher, J.H., Bourcier, W.L., Spadaccini, C.M., Lewis, J.A., Aines, R.D., 2015. Encapsulated liquid sorbents for carbon dioxide capture. Nat. Commun. 6, 1–7. doi:10.1038/ncomms7124.

Wilberforce, T., Baroutaji, A., Soudan, B., Al-Alami, A.H., Olabi, A.G., 2019. Outlook of carbon capture technology and challenges. Sci. Total Environ. 657, 56–72. doi:10.1016/j.scitotenv.2018.11.424.

Yu, C.-.H., 2012. A Review of CO_2 aaaaaaaaan. Aerosol Air Qual. Res. doi:10.4209/aaqr.2012.05.0132.

Yu, C., Huang, C., Tan, C., 2012. A review of CO_2 Capture by absorption and adsorption. Aerosol Air Qual. Res. 745–769. doi:10.4209/aaqr.2012.05.0132.

Zeng, S., Zhang, Xiangping, Bai, L., Zhang, Xiaochun, Wang, H., Wang, J., Bao, D., Li, M., Liu, X., Zhang, S., 2017. Ionic-Liquid-Based CO $_2$ capture systems: structure, interaction and process. Chem. Rev. 117, 9625–9673. doi:10.1021/acs.chemrev.7b00072.

Zhang, J., Chen, S., He, Q., Guo, P., Xu, Z., Zhang, D., 2018. Toughening benzoxazines with hyperbranched polymeric ionic liquids: effect of cations and anions. React. Funct. Polym. 133, 37–44. doi:10.1016/j.reactfunctpolym.2018.10.002.

Zhang, X., Xiong, W., Peng, L., Wu, Y., Hu, X., 2020. Highly selective absorption separation of H2S and CO2 from CH *4* by novel azole-based protic ionic liquids. AIChE J 66. doi:10.1002/aic.16936.

Zhang, X., Xiong, W., Shi, M., Wu, Y., Hu, X., 2021. Task-specific ionic liquids as absorbents and catalysts for efficient capture and conversion of H2S into value-added mercaptan acids. Chem. Eng. J. 408, 127866. doi:10.1016/j.cej.2020.127866.

Zhang, X., Xiong, W., Tu, Z., Peng, L., Wu, Y., Hu, X., 2019. Supported ionic liquid membranes with dual-site interaction mechanism for efficient separation of CO_2. ACS Sustain. Chem. Eng. 7, 10792–10799. doi:10.1021/acssuschemeng.9b01604.

Zulfiqar, S., Sarwar, M.I., Mecerreyes, D., 2015. Polymeric ionic liquids for CO_2 capture and separation: potential, progress and challenges. Polym. Chem. 6435–6451. doi:10.1039/C5PY00842E.